Taylor & Francis
Taylor & Francis Group

Philosophical Magazine

ISSN: 1478-6435 (Print) 1478-6443 (Online) Journal homepage: http://www.tandfonline.com/loi/tphm20

A crystal plasticity model of a formation of a deformation band structure

J. Kratochvíl & M. Kružík

To cite this article: J. Kratochvíl & M. Kružík (2015) A crystal plasticity model of a formation of a deformation band structure, Philosophical Magazine, 95:32, 3621-3639, DOI: 10.1080/14786435.2015.1090638

To link to this article: http://dx.doi.org/10.1080/14786435.2015.1090638

Philosophical Magazine, 2015
Vol. 95, No. 32, 3621–3639, http://dx.doi.org/10.1080/14786435.2015.1090638

A crystal plasticity model of a formation of a deformation band structure

J. Kratochvíl[ab*] and M. Kružík[bc]

[a]*Faculty of Mathematics and Physics, Charles University, Sokolovská 83, 186 75 Prague, Czech Republic;* [b]*Faculty of Civil Engineering, Department of Physics, Czech Technical University, Thákurova 7, 166 29 Prague, Czech Republic;* [c]*Department of Decision-Making Theory, Institute of Information Theory and Automation of the ASCR, Academy of Sciences of Czech Republic, Pod vodárenskou věží 4, 182 08 Prague, Czech Republic*

(*Received 28 January 2015; accepted 28 August 2015*)

The formation of deformation bands with the typically alternating sign of the misorientation across their boundaries is interpreted as spontaneous deformation instability caused by anisotropy of hardening. To analyse the nature of the fragmentation, a model of a rigid-plastic crystal domain deformed by symmetric double slip in a plane-strain compression is considered. The basic reason for the deformation band existence is that a local decrease in number of active slip systems in the bands is energetically less costly than a homogeneous deformation by multislip. However, such model of the bands predicts their extreme orientation and their width tends to zero. This trend is modified by hardening caused by a build up of the band boundaries and by a dislocation bowing (Orowan) stress. The model provides an explanation of observed orientation of the bands, their width and the significant change in the structural morphology seen as the band reorientation occurs at large strains. The predictions are in a favourable agreement with the available observations.

Keywords: deformation substructure; rigid-plastic crystal plasticity; spontaneous deformation instability; band orientation; band width

1. Introduction

Deformation bands are the basic microstructural elements in metal single crystals and polycrystals, where the dominating deformation mechanism is a dislocation glide. The deformation bands are detected in a form of elongated misoriented domains (cell blocks (CBs), microbands (MBs), lamellae, misoriented regions) separated by roughly parallel families of *geometrically necessary boundaries* (GNBs). While the deformation bands have been observed for decades, their importance as a potentially most valuable tool for understanding the mechanism of plastic deformation has only come to light relatively recently (the reviews, e.g. [1–4]). From the continuum mechanics point of view, the deformation and shear bands are spontaneous deformation instabilities [5,6]; Biot [5] called them the internal buckling. The nature of the shear and deformation bands is different. The shear bands arise from a material softening (including geometrical softening [7]). The deformation bands are a

*Corresponding author. Email: kratochvil@fsv.cvut.cz

consequence of anisotropy of hardening. The anisotropy causes that it is energetically less costly to flow the material through the crystal lattice buckled by the deformation bands with a decreased number of the active slip systems than to flow it through a lattice deformed homogeneously by multislip.

The inner structure built in the deformation bands to facilitate the plastic flow depends on the character of slip. In cell-forming metal single crystals and polycrystals (medium to high stacking fault energy crystalline materials with easy cross-slip), at moderate strain (von Mises strain $\varepsilon \sim 0.3$–0.7 in rolled Al), most often the deformation band substructure consists of one or two sets of the extended sharp planar GNBs with a specific crystallographic alignment between which fairly equiaxed cells are formed [1,4,8], Figure 1 The deformation bands termed *cell blocks* are defined as a contiguous group of cells in which the same set of glide systems operate.

As observed by Hughes [9], in the rolled Al–Mg, the framework for a crystal domain subdivision in non-cell-forming metals is analogous to that observed in the cell-forming metals. The principal difference is that the inner substructure of the deformation bands (termed misoriented regions) consists of the dislocations organised into a Taylor lattice containing multiple Burgers vectors and having the alternating misorientation along the [1 1 1] slip plane. Unlike the rather sharp GNBs, in the cell-forming metals the GNBs observed in the Al–Mg are diffuse.

A typical microstructural evolution during rolling of fcc medium to high stacking fault energy metals has been analysed in detail by Hughes and Hansen in [10,11]. The deformation microstructures evolved in high purity nickel cold-rolled from 0.5 to 4.5 von Mises effective strain were observed and analysed. The special emphasis was focused on factors that contribute to the transition from structures characteristic of small to medium strain microstructures to those characteristic to large strain microstructures. The observations reported in [10,11] can be summarised as follows.

At small strains, the GNBs bounding CBs are long *dense dislocation walls* (DDWs) with a specific macroscopic orientation with respect to the rolling direction (RD). The spacing between the DDWs decreases with increasing strain by the creation of new DDWs within the CBs and the misorientations across DDWs increase. The requirement of strain compatibility across the DDWs is met through further subdivision at the DDWs. Subdivision occurs by creating thin plate-like CBs at the DDWs. The new CBs have been defined as *microbands*. The thickness of the MBs ranges from 0.1 to 0.4 μm.

At intermediate strain, in addition to the MBs and DDWs, there have been observed bands of intense local crystallographic slip labelled as *S-bands*. They intersect parallel groups of MBs creating on them a string of "S"-shaped perturbations. The passage of regularly distributed S-bands causes a large-scale reorganisation of the original MBs and CBs microstructure to a *lamellar structure* oriented at shallow angles to the RD. The transition from a microstructure composed of MBs and DDWs to one composed of lamellae occurs gradually over a very large strain range from an effective strain of 0.5–3. At the very high effective strain of 4.5, no remaining MBs were observed. At large strains ($\varepsilon > 2$), the lamellae with more or less alternating rotations dominate the microstructure. The angle between the lamellae and the RD decreases with the increasing degree of deformation being only a few degrees after 90% cold rolling. However, the lamellae are never parallel to the rolling plane [10]. The lamellae are grouped in the bands which have a width of 0.5-3 μm. At very high strains, the spacing between the deformation-induced boundaries can reach the order of 100 nm.

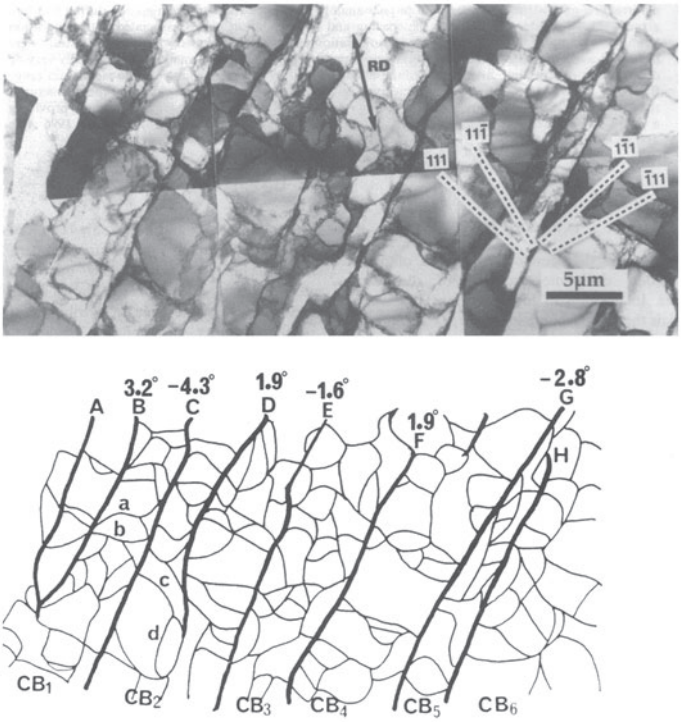

Figure 1. (a) The electron micrograph from a plane containing the rolling and normal directions of pure aluminium; cold-rolled 10%; (b) the sketch of the microstructure [12].

An example of the dislocation microstructure developed during rolling in a cell-forming metal is shown in Figure 1 [12]. The microstructure is subdivided by the GNBs marked A, B, C, …bounding CBs containing dislocation cells marked a, b, c, …; the RD is marked by RD. The numbers indicate the alternating misorientation across the GNBs. The detailed characterisation of the dislocation composition within the GNBs nearly aligned with the two activated slip planes in pure aluminium cold-rolled 10% was presented by Hong et al. [8,13] (at larger strains individual dislocations were not clearly visible). The dislocations with all six Burgers vectors of the <1 1 0>/2 type expected for fcc crystals were observed, however, the dislocations from the four most active slip systems dominated. It was found that most of the dislocations were well organised into a reasonably flat two-dimensional network. The measurements were done in the polycrystalline grains oriented nearly symmetrically with respect to the rolling plane and the RD (the rotated cubic orientation). The orientation of the two active f.c.c. slip planes symmetrically oriented with respect to the rolling plane in the plane-strain approximation is ±55°. From the mechanics point of view, the grains can be considered approximately as exposed to a plain strain compression carried by the two symmetrical sets of coplanar slip systems oriented ±35° with respect to the direction of compression analysed in the present paper.

According to Harren et al., experiments on Al–Cu single crystals exposed to a plane-strain compression [14], the observed (1 1 0)[0 0 1] geometry coincides with a stable state of symmetric slip on the four slip systems as detected by Hong et al. [8,13]: the directions

$[1\,0\,\bar{1}]/2$ and $[0\,1\,\bar{1}]/2$ in the $(1\,1\,1)$ plane and the directions $[1\,0\,1]/2$ and $[0\,1\,1]/2$ in the $(1\,1\,\bar{1})$ plane. The net shearing systems associated with this symmetric state are then the $[1\,1\,\bar{2}]$ in the $(1\,1\,1)$ and the $[1\,1\,2]$ in the $(1\,1\,\bar{1})$. In order to simulate the compression tests of the single crystals, Harren et al. [14] employed a two-dimensional single crystal model with two considered slip systems $(1\,1\,1)[1\,1\,\bar{2}]$ and $(1\,1\,\bar{1})[1\,1\,2]$. The orientation of the slip systems with respect to the compression axis is $\phi = 35°$. The experimental observations and the computed deformation response have been in a close agreement. Inspired by Harren's et al. successful approach [14], we use the idealised model of the two-dimensional plane-strain compression in modelling of some observed properties of the deformation bands. The plane-strain model has been employed already in the previous publications [15–17] in the attempts to analyse the formation of the cell substructure. Here, we use mainly the papers [18–20] recalled in the next Section as a starting point of our considerations.

The modelling is based on the mechanics of incremental deformations proposed by Biot [5]. Biot's theory provides rigorous and completely general equations governing the dynamics and stability of solids and fluids under an initial stress in the context of small perturbations. The method allows using the linear theory of the incremental deformations even for the analysis of advance stages of deformation. The main idea of the method is to expose the crystal domain in a given deformation state of a stress $\bar{\sigma}$ and a strain ε to an incremental, generally inhomogeneous deformation mode and to evaluate the incremental work needed to carry the deformation. The lowest incremental work indicates the preferred mode which will dominate the evolving deformation substructure. We employ Biot's theory of instability modes of orthotropic materials, where the orthrotropy is carried by symmetric double slip with distinguished latent hardening.

Biot [5], in his analysis, was probably the first who treated the deformation bands (his instability of the first kind) as a consequence of material anisotropy. A comprehensive review of continuum mechanic approaches to the deformation banding has been given by Petryk and Kursa [21]. A constitutive framework for elastic-plastic finite deformation has been formulated by Hill [22], Hill and Rice [23], and widely applied in the study of formation of shear bands e.g., [7,24,25]. The model of deformation banding developed by Ortiz et al. [26,27] is based on incremental minimisation of the pseudo-elastic energy. They assumed that the corresponding energy densities undergoing latent hardening are non-convex with energy preference for single slip. Such incremental energy potential exists locally if the deformation field is split into compatible domains of single slip on different slip systems. In computations, such splitting was enforced by assuming infinite latent hardening [28]. However, in general, for multiple slip, the governing rate equations cannot be cast in a variational form as the hardening matrix may be non-symmetric.

In some of most advanced theoretical investigations, Petryk et al. [21,29–32] aimed to clarify formulation and justification of the incremental energy criterion for deformation banding in crystals deformed locally by multislip. In the criterion for incipient deformation banding, the key role is played by symmetrisation of the hardening submatrix restricted to the active slip systems in the energy minimisation solution. Additionally, the second-order minimisation has been extended to a finite time step in order to enable numerical calculation of the initial modes of deformation banding and tracing deformation paths under external control. In view of this, an attempt has been made to simulate the deformation band pattern under tension with the focus on predicting three distinct microstructure types observed in three different domains of the tensile axis orientation [33,34]. The simplified model introduced in the next Sections presents an essence of the energetic approach of

Petryk–Kursa's type. We employ the simplest approach to reveal mechanisms responsible for deformation banding and their observed features as described above. We use the original Biot's model [5] modified for crystal plasticity and enriched with the length scale effects. The orthotropy of the model induced by the assumption of symmetric double slip guarantees the symmetry of the hardening matrix, which enables a variational formulation and the energy minimisation process.

Two other attempts to interpret some features of deformation bands have been proposed. Mahesh [35] suggested a hypothesis based on the three physical principles that determine the preferred CB boundary orientation in the rigid-plastic model of an arbitrarily oriented grain of a polycrystal: (i) a uniform state of stress prevails throughout the grain; (ii) the CBs are disoriented so as to minimise the power of plastic deformation; and (iii) the CB boundaries are oriented so as to minimise plastic incompatibility between the neighbouring CBs. The predicted orientations and disorientations have been compared favourably with those reported in the experimental literature. Winther [36,37] calculated the dislocation configuration in the GNBs and its misorientation by means of the principle of low-energy dislocation structures assuming the boundaries free of long-range stresses. Following Leffers [38,39], the misorientations across the boundaries were evaluated using a continuum mechanics condition that at the boundaries between the neighbouring CBs with different slip system activities must remain in contact.

In the next Section, a symmetric double slip model of a spontaneous formation of the deformation bands is presented in a variational form suitable for an energetic consideration. In the Section 2.1 we adopt the rigid-plastic, rate-independent approximation, which turns out to be the optimal viewpoint pointing to the essential features of the formation of the deformation bands. The model is constructed in two steps. A simple version of the model based on the standard hardening rule, Section 2.2, reveals the conditions for the formation of the deformation bands. In the next step, except for modification of the hardening rule (the equations (23) and (24) in the Section 2.3), which incorporates additionally a hardening caused by the incremental work needed to build up the boundaries and to overcome the dislocation bowing stress, we follow the classical crystal plasticity framework. The results provide an interpretation of the band orientation, their width, the misorientation across the band boundaries, their dislocation composition and the band reorientation occurring at large strains. A preliminary version of the model has been outlined in [40].

2. Rigid-plastic model of symmetric double slip

We consider a plane-strain deformation of an infinitely extended rigid-plastic crystal domain in the coordinate system (x, y), Figure 2. The plane-strain compression simulating a rolling process is assumed to be homogeneous up to a certain deformation level. The deformation increment at this point can be either homogeneous again, or else, it can be inhomogeneous. The aim of this analysis is to determine under which conditions the deforming crystal domain prefers an inhomogeneous increment in the form of deformation bands. The considered symmetric double-slip compression with the symmetry axis coinciding with the y coordinate axis is a convenient two-dimensional idealisation of a crystal domain symmetrically oriented with respect to the normal direction of the rolling plane (rotated cubic orientation), as seen in Figure 2. The angle of the slip planes with respect to the y axis is $\phi = 35°$.

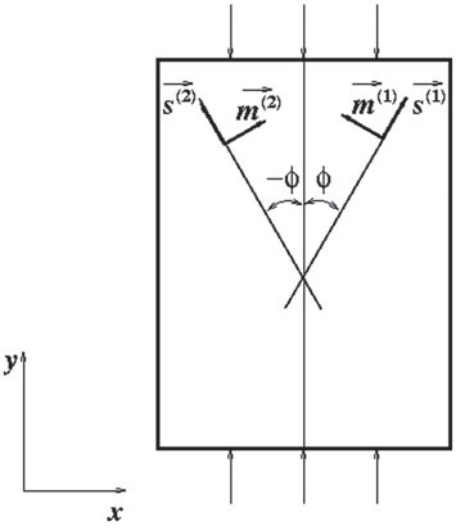

Figure 2. Symmetric double slip in plane-strain compression.

2.1. *Kinematics*

The incremental deformation representing a deviation from the original symmetric double slip is expressed through an incremental displacement vector $\hat{\boldsymbol{u}}(x, y)$. The displacement gradient $\nabla\hat{\boldsymbol{u}}$ can be decomposed into a plastic part, which represents the material flow carried by dislocations and an elastic part. In the rigid-plastic approximation, the elastic part reduces to an increment of a rigid rotation of the crystal lattice $\hat{\boldsymbol{\omega}}^*$. For small increments the decomposition reads $\nabla\hat{\boldsymbol{u}} = \hat{\boldsymbol{\beta}} + \hat{\boldsymbol{\omega}}^*$, where the increment of the plastic distortion $\hat{\boldsymbol{\beta}}$ caused by incremental slips $\hat{\gamma}^{(1)}(x, y)$ and $\hat{\gamma}^{(2)}(x, y)$ on the two considered slip systems, Figure 2, reads

$$\hat{\boldsymbol{\beta}} = \sum_{i=1}^{2} \hat{\gamma}^{(i)} \boldsymbol{s}^{(i)} \otimes \boldsymbol{m}^{(i)}\,, \tag{1}$$

$\boldsymbol{s}^{(1)} = (\sin\phi, \cos\phi)$ and $\boldsymbol{s}^{(2)} = (-\sin\phi, \cos\phi)$ represent the slip directions, and $\boldsymbol{m}^{(1)} = (-\cos\phi, \sin\phi)$ and $\boldsymbol{m}^{(2)} = (\cos\phi, \sin\phi)$ are the unit slip plane normals; $\pm\phi$ is the orientation angle of the slip planes with respect to the symmetry axis of the compression.

The incremental strain $\hat{\boldsymbol{\varepsilon}}(x, y)$ superposed upon the current homogeneous strain $\boldsymbol{\varepsilon}$ is defined as $\hat{\boldsymbol{\varepsilon}} = \left(\nabla\hat{\boldsymbol{u}} + \left(\nabla\hat{\boldsymbol{u}}\right)^T\right)/2$. For the model considered one can deduce from (1)

$$\hat{\varepsilon}_{xx} = -\hat{\varepsilon}_{yy} = -\sin 2\phi\,\left(\hat{\gamma}^{(1)} + \hat{\gamma}^{(2)}\right)/2\,, \qquad \hat{\varepsilon}_{xy} = -\cos 2\phi\,\left(\hat{\gamma}^{(1)} - \hat{\gamma}^{(2)}\right)/2\,. \tag{2}$$

The increments of the lattice rotation $\hat{\omega}^*$, representing the lattice misorientation, is related to the increments of the material rotation $\hat{\omega} = \hat{\omega}_{xy} = \left(\partial_y\hat{u}_x - \partial_x\hat{u}_y\right)/2$ and the plastic rotation $\hat{\omega}^p = \left(\hat{\gamma}^{(1)} - \hat{\gamma}^{(2)}\right)/2$ as $\hat{\omega}^* = \hat{\omega} - \hat{\omega}^p$. In general, the elastic and plastic parts of the incremental deformation $\nabla\hat{\boldsymbol{u}}$ may be individually incompatible. The incremental density of the geometrically necessary dislocations (GNDs) required for the deformation

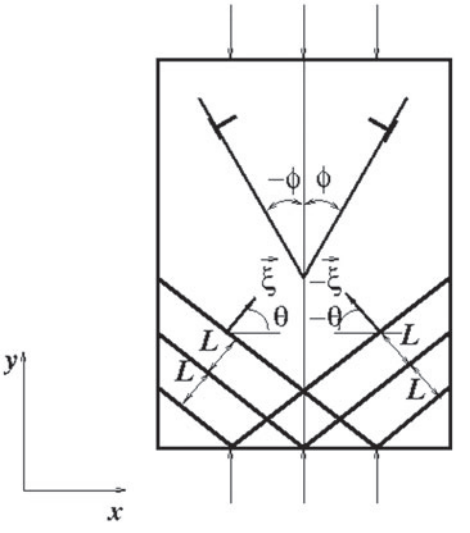

Figure 3. Scheme of two sets of deformation bands perpendicular to the vectors $\pm\boldsymbol{\xi}$, L is the band width.

to remain compatible is characterised by the increment of the dislocation density tensor $\hat{\boldsymbol{\alpha}} = \operatorname{curl}\hat{\boldsymbol{\beta}} = -\operatorname{curl}\hat{\boldsymbol{\omega}}^*$ that reveals the relation between the misorientation of the crystal lattice $\hat{\boldsymbol{\omega}}^*$ and the dislocation density of GNDs measured by the tensor $\hat{\boldsymbol{\alpha}}$. Here, and in the sequel, the curl of a tensor is defined as the curl of rows of the tensor. The tensor $\hat{\boldsymbol{\alpha}}$ can be resolved into the dislocation incremental densities $\hat{\boldsymbol{\alpha}}^{(i)}$, $i = 1, 2$, of GNDs of the individual slip systems,

$$\hat{\boldsymbol{\alpha}} = \hat{\boldsymbol{\alpha}}^{(1)} + \hat{\boldsymbol{\alpha}}^{(2)} = \sum_{i=1}^{2} \operatorname{curl}\hat{\boldsymbol{\beta}}^{(i)} = \sum_{i=1}^{2} \operatorname{curl}\left(\hat{\gamma}^{(i)}\boldsymbol{s}^{(i)} \otimes \boldsymbol{m}^{(i)}\right). \tag{3}$$

The tensors $\hat{\boldsymbol{\alpha}}^{(i)}$ specify the GNBs dislocation composition in the plane-strain approximation; in the coordinate system of Figure 2, the matrices of the density tensor increments $\hat{\boldsymbol{\alpha}}^{(i)}$ are reduced to the single non-zero components

$$\hat{\alpha}^{(1)} = (\sin\phi\,\partial_x + \cos\phi\,\partial_y)\hat{\gamma}^{(1)}, \quad \hat{\alpha}^{(2)} = (-\sin\phi\,\partial_x + \cos\phi\,\partial_y)\hat{\gamma}^{(2)}. \tag{4}$$

As for boundary conditions, we consider an infinitely extended crystal domain and assume periodicity in x and y directions of all the incremental fields. For instance,

$$\hat{\boldsymbol{\varepsilon}}(x, y) = \hat{\boldsymbol{\varepsilon}}(x + L_x, y + L_y), \tag{5}$$

where L_x and L_y are the length of one period in the corresponding directions. Since the lengths L_x and L_y can be extended to infinity, the periodicity is only a formal requirement. It enables us to get rid of the boundary terms that would otherwise appear when applying Green's theorem in the integral formulation (18).

Next, we introduce the stream function ψ by the relations $\hat{u}_x = \partial_y\psi$, $\hat{u}_y = -\partial_x\psi$ which guarantee incompressibility $\operatorname{tr}\hat{\varepsilon} = 0$. We look for an inhomogeneous, kinematically

admissible deformation increment, which can be constructed from the stream function ψ in the form

$$\psi = F(x + \xi y)\,, \tag{6}$$

which represents an inhomogeneous simple shear parallel to the planes $x + \xi y =$ constant. The shear inhomogeneity can be interpreted as a deformation band-like pattern perpendicular to the direction $\xi = \tan\theta$, where θ is the angle between the x axis and the normal to the bands, Figure 3.[1] In view of the linearity of the problem at hand, any linear combination of the stream functions of the type (6) with different profiles F and directions ξ is kinematically admissible. The kinematically admissible strain and rotation are derived by means of the stream function ψ and the kinematic relations $\hat{\boldsymbol{\varepsilon}} = \left(\nabla\hat{\boldsymbol{u}} + \left(\nabla\hat{\boldsymbol{u}}\right)^T\right)/2$ and $\hat{\omega} = \left(\nabla\hat{\boldsymbol{u}} - \left(\nabla\hat{\boldsymbol{u}}\right)^T\right)/2$ (F'' represents the second derivative with respect to the argument $x + \xi y$)

$$\hat{\varepsilon}_{xx} = -\hat{\varepsilon}_{yy} = \xi F''\,, \quad \hat{\varepsilon}_{xy} = \frac{1}{2}\left(\xi^2 - 1\right)F''\,, \quad \hat{\omega} \equiv \hat{\omega}_{xy} = \frac{1}{2}\left(\xi^2 + 1\right)F''\,. \tag{7}$$

Kinematically admissible crystallographic slip increments then result from (2),

$$\hat{\gamma}^{(1)} = \left(\frac{1-\xi^2}{2\cos 2\phi} - \frac{\xi}{\sin 2\phi}\right)F''\,, \quad \hat{\gamma}^{(2)} = \left(\frac{\xi^2-1}{2\cos 2\phi} - \frac{\xi}{\sin 2\phi}\right)F''\,, \tag{8}$$

and using (4) we get for the increments of the dislocation densities

$$\begin{aligned}\hat{\alpha}^{(1)} &= (\sin\phi + \xi\cos\phi)\left(\frac{1-\xi^2}{2\cos 2\phi} - \frac{\xi}{\sin 2\phi}\right)F'''\,,\\ \hat{\alpha}^{(2)} &= (-\sin\phi + \xi\cos\phi)\left(\frac{\xi^2-1}{2\cos 2\phi} - \frac{\xi}{\sin 2\phi}\right)F'''\,.\end{aligned} \tag{9}$$

The increment of the alternating lattice misorientation $\hat{\omega}^*$ and the incremental plastic rotation $\hat{\omega}^p$ are expressed as

$$\hat{\omega}^* = \frac{\left(\xi^2+1\right)\cos 2\phi + \xi^2 - 1}{2\cos 2\phi}F''\,, \quad \hat{\omega}^p = \left(\hat{\gamma}^{(1)} - \hat{\gamma}^{(2)}\right)/2 = \left(\frac{1-\xi^2}{2\cos 2\phi}\right)F''\,. \tag{10}$$

2.2. *The simple model*

The simple version of the model partly analysed in [18,40] is Biot's original model [5] adopted to crystal plasticity of the plane-strain symmetric double slip. The model provides the basic result of the energetic approach: the existence of the deformation bands. As it will be shown at the end of this Section, the predicted bands in the simple case have extremal properties: the orientation is perpendicular to the direction of the compression and their width tends to zero.

The stress $\boldsymbol{\sigma}$ in the deforming crystal domain expressed in a reference frame which rotates with the crystal lattice consists of three contributions

$$\boldsymbol{\sigma} = \bar{\boldsymbol{\sigma}} + \hat{\boldsymbol{\sigma}} + \hat{\boldsymbol{\omega}}^p\bar{\boldsymbol{\sigma}} + \bar{\boldsymbol{\sigma}}\left(\hat{\boldsymbol{\omega}}^p\right)^{\mathrm{T}}. \tag{11}$$

$\bar{\boldsymbol{\sigma}}$ is the applied homogeneous stress, which, in a given state of the plastic regime has a character of a pre-stress. In the considered case of the plane-strain compression, the stress

$\bar{\boldsymbol{\sigma}}$ has a single component, $\bar{\sigma} < 0$, in the y direction as shown in Figure 2. The term $\hat{\boldsymbol{\omega}}^p \bar{\boldsymbol{\sigma}} + \bar{\boldsymbol{\sigma}} \left(\hat{\boldsymbol{\omega}}^p\right)^{\mathrm{T}}$ accounts for the geometrical hardening/softening, i.e. for a change in the stress due to the rotation of the pre-stress tensor with respect to the crystal lattice. The incremental stress $\hat{\boldsymbol{\sigma}}$ is related to the incremental slips $\hat{\gamma}^{(i)}$ by the constitutive equations.

The slip increments are induced by the increments in the resolved shear stresses $\hat{\tau}^{(i)} = \boldsymbol{s}^{(i)} \cdot \hat{\boldsymbol{\sigma}}\, \boldsymbol{m}^{(i)}$, $i = 1, 2$, that result as

$$\hat{\tau}^{(1)} = -\sin 2\phi \left(\hat{\sigma}_{xx} - \hat{\sigma}_{yy}\right)/2 - \cos 2\phi \hat{\sigma}_{xy}\,, \quad \hat{\tau}^{(2)} = -\sin 2\phi \left(\hat{\sigma}_{xx} - \hat{\sigma}_{yy}\right)/2 + \cos 2\phi \hat{\sigma}_{xy}\,. \tag{12}$$

In the rate-independent approximation, the resolved shear stress equals the flow stress in the plastic regime. This is accounted for the hardening rule representing the constitutive equations of the simple model,

$$\hat{\tau}^{(1)} = h\,\hat{\gamma}^{(1)} + qh\,\hat{\gamma}^{(2)}\,, \quad \hat{\tau}^{(2)} = qh\,\hat{\gamma}^{(1)} + h\,\hat{\gamma}^{(2)}\,. \tag{13}$$

The entries are the self-hardening coefficient h and the latent (cross) hardening coefficient qh. The latent-to-active hardening ratio q is a measure of the hardening anisotropy. It is one of the key parameters of the model.

The equations (2), (11)–(13) lead to the incremental constitutive relations for an orthotropic, incrementally-linear rigid-plastic solid in the form proposed by Biot [5], namely

$$\hat{\sigma}_{xx} - \hat{\sigma}_{yy} = 2H_{xx}\left(\hat{\varepsilon}_{xx} - \hat{\varepsilon}_{yy}\right)\,, \quad \hat{\sigma}_{xy} = 2H_{xy}\hat{\varepsilon}_{xy}\,, \tag{14}$$

where the instantaneous hardening coefficients are

$$H_{xx} = \frac{h(1+q)}{2\sin^2 2\phi}\,, \quad H_{xy} = \frac{h(1-q) + \bar{\sigma}\cos 2\phi}{2\cos^2 2\phi}\,. \tag{15}$$

The incremental stress $\hat{\boldsymbol{\sigma}}$ has to satisfy the condition of the equilibrium for a pre-stressed domain [5] expressed in the terms of the (objective) corotational derivative of the Cauchy stress increment

$$\begin{aligned} \partial_x \hat{\sigma}_{xx} + \partial_y \hat{\sigma}_{xy} + \bar{\sigma}\,\partial_y \hat{\omega} &= 0\,, \\ \partial_x \hat{\sigma}_{xy} + \partial_y \hat{\sigma}_{yy} + \bar{\sigma}\,\partial_x \hat{\omega} &= 0\,. \end{aligned} \tag{16}$$

For the purpose of the energy considerations, the problem is cast in terms of a variational formulation.

We utilise the principle of virtual displacements, $\int \mathrm{div}\hat{\boldsymbol{\sigma}} \cdot \delta\hat{\boldsymbol{u}} = 0$, that is

$$\int_\Omega \left(\left(\partial_x \hat{\sigma}_{xx} + \partial_y \hat{\sigma}_{xy} + \bar{\sigma}\,\partial_y \hat{\omega}\right)\delta\hat{u}_x + \left(\partial_x \hat{\sigma}_{xy} + \partial_y \hat{\sigma}_{yy} + \bar{\sigma}\,\partial_x \hat{\omega}\right)\delta\hat{u}_y\right)\mathrm{d}V = 0\,, \tag{17}$$

where Ω is the crystal domain in the xy plane and $\delta\hat{\boldsymbol{u}}(x, y)$ is an arbitrary virtual displacement field. By using Green's theorem and the chosen periodic boundary conditions we get the weak form of the equilibrium equation (16)

$$\int_\Omega \left(\hat{\sigma}_{xx}\delta\hat{\varepsilon}_{xx} + 2\left(\hat{\sigma}_{xy} + \bar{\sigma}\,\hat{\omega}\right)\delta\hat{\varepsilon}_{xy} + \hat{\sigma}_{yy}\delta\hat{\varepsilon}_{yy}\right)\mathrm{d}V = 0\,. \tag{18}$$

Introducing the constitutive relation (14) into (18), expressing $\hat{\varepsilon}_{xx}, \hat{\varepsilon}_{yy}, \hat{\varepsilon}_{xy}$ and $\hat{\omega}$ through the stream function, the relations (7) and using the symmetry of hardening (13),

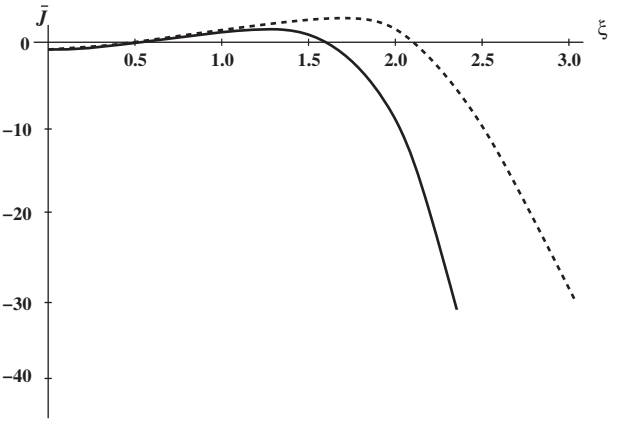

Figure 4. Graph of the reduced energetic functions $\bar{J}(\xi)$, (the full line); ξ characterises the band orientation. The dashed line represents the reduced function where the pre-stress $\bar{\sigma} = 0$; it demonstrates a destabilising effect of $\bar{\sigma}$; as seen, for $\bar{\sigma} = 0$ the range of the stability $\bar{J}(\xi) > 0$ has been extended.

the weak form of the equilibrium (18) can be expressed as an extreme of the functional J requiring its first variation to be zero, $\delta J = 0$,

$$J = \frac{1}{2}\int_\Omega \left(4H_{xx}\xi^2 + H_{xy}\left(\xi^2 - 1\right)^2 - \frac{\bar{\sigma}}{2}\left(1 - \xi^4\right)\right)\left(F''\right)^2 \,\mathrm{d}V\,. \tag{19}$$

The inhomogeneous incremental deformation defined by $F(x+\xi y) \neq 0$, the equation (6), is now assumed to be such a deviation from a homogeneous increment, that the corresponding strains vanish on average. A homogeneous increment can be formally represented by $F(x + \xi y) = 0$. The functional (19) thus now represents an energy difference between the homogeneous and inhomogeneous deformation increments. The inhomogeneous deformation increment is energetically favourable if the functional (19) becomes negative, $J < 0$. If a kinematically possible deformation exists that fulfils this condition, then the homogeneous deformation is unstable and a pattern is formed. Since $\left(F''\right)^2$ in (19) is positive, the sign of J is determined by the sign of the energetic function $4H_{xx}\xi^2 + H_{xy}\left(\xi^2 - 1\right)^2 - \bar{\sigma}\left(1 - \xi^4\right)/2$. In view of (15) this function may become negative for $h > 0$ and $q > 1$, i.e. a dominant latent hardening, further assisted by the compression $\bar{\sigma}$. This is demonstrated by the graph of the reduced energetic function $\bar{J}(\xi) = J(\xi)/H_{xx}\int\left(F''\right)^2$, the full line in Figure 4,

$$\bar{J}(\xi) = 2\xi^2 + K\left(1 - \xi^2\right)^2 + S\left(1 - \xi^4\right)\,, \tag{20}$$

where

$$K = H_{xy}/2H_{xx} = \frac{h(1-q) + \bar{\sigma}\cos 2\phi}{2h(1+q)}\tan^2 2\phi\,, \quad S = \frac{\bar{\sigma}}{4H_{xx}} = \frac{\bar{\sigma}}{2h(1+q)}\sin^2 2\phi. \tag{21}$$

The graphs of $\bar{J}(\xi)$ were evaluated for $\phi = 35°$, the self-hardening $h = 400\,\mathrm{MPa}$, $q = 1.5$ and the compressive flow stress $\bar{\sigma} = -500\,\mathrm{MPa}$ deduced from the stress–strain

diagram of nickel at the moderate strain $\varepsilon = 0.5$ in [4] (Fig. 14). In view of the symmetry of $\bar{J}(\xi)$ with respect to the origin, we discuss only the case $\xi > 0$. In the central part, the function $\bar{J} > 0$, so that the forming of a pattern would be energetically costly. On the other hand, in the other parts there is the energy gain in forming the pattern. The inhomogeneous incremental deformation with $\xi \to \infty$ is the most energetically favourable. It corresponds to the deformation band-like pattern perpendicular to the y-axis, $\theta \to \pi/2$ (parallel to the RD).

Note that such solution satisfies compatibility, but not necessarily the stress equilibrium (16). The equilibrium is guaranteed only for $2\xi^2 + K(1-\xi^2)^2 + S(1-\xi^4) = 0$, which is the characteristic equation of the weak form of the stress equilibrium $\delta J = 0$. These solutions are represented by the cross section points on ξ axis in Figure 4. In the paper [18] it has been proved for $S = 0$ that these equilibrium solutions are just marginally stable or energetically neutral indicating a tendency to reach the solution $\xi \to \infty$ as shown in Figure 4.

To estimate a length scale of the pattern, we consider the deformation banding inspired by a band substructure observed in the cell-forming metals, i.e. the periodically arranged deformation bands perpendicular to the direction ξ separated by the sharp GNBs. The bands of the width L are assumed to be homogeneously sheared, i.e. $F'' = \pm(a/L)$, where a is an amplitude of the incremental displacement. Under these assumptions, the functional (19) integrated over the crystal domain Ω becomes a function

$$J(\xi, L) = \frac{1}{2}\left(4H_{xx}\xi^2 + H_{xy}\left(\xi^2 - 1\right)^2 - \frac{\bar{\sigma}}{2}\left(1 - \xi^4\right)\right)\frac{a^2}{L^2}V\,, \tag{22}$$

where V is the volume of the crystal domain Ω. As will be shown in the next Section 2.3, the function (22) is a special case of more general energetic function (29) if the length-scale effects are neglected. The function (22) indicates that for a given amplitude a the fastest growth of the pattern is reached for $L \to 0$.

That the deformation bands tend to be oriented perpendicularly to the compression direction and to have a zero width was discovered by Biot [5]. He noted ([5] p.199):

> This conclusion may seem paradoxical, but there are inherent limitations in the validity of the theory for very small wavelengths. It is, of course, not valid in the atomic scale. Then non-linearity also enters into play. The result therefore indicates that the buckling wavelength will tend to be the smallest compatible with the small-scale physics of the medium.

In our consideration, in Section 2.3 a proposed small-scale physics is the resistance of the GNBs to slip and the work needed to overcome the dislocation bowing stress.

2.3. *The model enriched with length-scale effects*

To describe more realistically the deformation bands orientation, their reorientation and their width the model has to be enriched with additional features. The shrinking width of the bands decreases the space for the dislocation glide, hence, their bowing stress grows causing a line tension (Orowan) strengthening. To build up the GNBs requires additional work needed to overcome the boundary resistance to slip. These effects can be incorporated in the model by a modification of the hardening rule.

The proposed rule consists of two parts: a bulk part $\hat{\tau}_V^{(i)}$ and a boundary part $\hat{\tau}_B^{(i)}$. The bulk part is assumed in the form

$$\hat{\tau}_V^{(1)} = (h + h_{\text{bow}})\,\hat{\gamma}^{(1)} + qh\,\hat{\gamma}^{(2)}\,, \quad \hat{\tau}_V^{(2)} = qh\,\hat{\gamma}^{(1)} + (h + h_{\text{bow}})\,\hat{\gamma}^{(2)}\,, \tag{23}$$

where a hardening term h_{bow} is added to the self-hardening part of the standard rule (13). The reason is that the dislocation bowing hinders the active slip, but causes no additional latent hardening. We employ a standard form of the line tension strengthening $h_{\text{bow}} = 2\sin\beta_c\, Gb/d$, where the critical angle β_c characterises the penetrability of obstacles and d is the distance between obstacles causing the dislocation bowing. G is the shear modulus and b the magnitude of the Burgers vector. In the present context the prominent obstacles are most probably the cell boundaries formed within the deformation bands. The cell size changes in a monotonic way with the changing width of the bands. Therefore, the distance d is identified with the band width L. In the present model, we assume a partial penetrability of the boundaries assuming that $h_{\text{bow}} = Gb/L$.

The boundary part of the modified hardening rule represents a complex problem: at boundaries dislocations can be reflected, absorbed or desorbed and/or transmitted directly. Here we employ a phenomenological approach. There are two possibilities: the GNBs can be modelled using gradients of dislocation densities or to treat the GNBs as planar interfaces.

In general, work hardening is controlled by dislocation interactions. The interactions are non-local and they should be expressed in an integral form. In the statistical considerations [20] only two types of interaction terms of the expansion of such integrals have been retained: the standard local hardening (13) that depends on the so-called statistically distributed dislocations and a non-local hardening which expresses that the resistance to the dislocation motion depends also on the arrangement of the dislocations. The gradients of the GND density increments $\hat{\alpha}^{(i)}$, $i = 1, 2$, given by (3) or (9) can be taken as simplified characteristics of the changes in that arrangement. The dislocation density gradients could be suitable for a simulation of the diffuse GNBs as observed in non-cell-forming metals [9] (a gradient version of the hardening rule will be analysed in a forthcoming paper). For the sharp GNBs in cell-forming metals considered here, it seems to be more realistic to treat the GNBs as planar interfaces.

The GNBs as interface objects are characterised by a matrix of the boundary part of the flow rule in an analogy to the standard anisotropic hardening (13)

$$\hat{\tau}_B^{(1)} = \tilde{h}\,\Delta\hat{\gamma}^{(1)} + \tilde{q}\tilde{h}\,\Delta\hat{\gamma}^{(2)}\,, \quad \hat{\tau}_B^{(2)} = \tilde{q}\tilde{h}\,\Delta\hat{\gamma}^{(1)} + \tilde{h}\,\Delta\hat{\gamma}^{(2)}\,. \tag{24}$$

The terms in (24) can be interpreted as a part of the flow stress increments needed to penetrate a cluster of the GNDs of the same ($\tilde{h}$) or the other slip system ($\tilde{q}\tilde{h}$). The jumps $\Delta\hat{\gamma}^{(i)}$, $i = 1, 2$, represent the difference in the slip increments across the GNBs between the neighbouring bands. $\Delta\hat{\gamma}^{(i)}$ are proportional to the net increments of the corresponding densities of the dislocations absorbed at the GNBs.

To get a modified energy functional J_c, one can follow the procedure represented by (17)–(19), where in (19) the increments $\hat{\boldsymbol{\varepsilon}}$ and $\hat{\boldsymbol{\sigma}}$ are expressed through (2) and (12) in terms of the increments $\hat{\gamma}^{(i)}$ and $\hat{\tau}^{(i)}$. Then, employing the flow rules (23) and (24), we get

$$J_c = 2\int_\Omega \left\{\left(h + h_{\rm bow}\right)\left[\left(\gamma^{(1)}\right)^2 + \left(\gamma^{(2)}\right)^2\right] + 2qh\,\gamma^{(1)}\gamma^{(2)} + \frac{\bar\sigma}{2}\left(\gamma^{(1)} - \gamma^{(2)}\right)\left(\gamma^{(1)} - \gamma^{(2)} + \omega\right)\right\} {\rm d}V + 2\int_A \left\{\tilde h\left[\left(\Delta\gamma^{(1)}\right)^2 + \left(\Delta\gamma^{(2)}\right)^2\right] + 2\tilde q\tilde h\left(\Delta\gamma^{(1)}\right)\left(\Delta\gamma^{(2)}\right)\right\} {\rm d}A\,, \tag{25}$$

where dV is a volume element of the crystal domain Ω and dA a surface element of the set A of GNBs contained in the domain.[2]

Similarly, as in the case of the simple model, we assume that the set of the deformation modes to be optimised is restricted to structures arising from superposition of one or two periodically arranged sets of parallel deformation bands perpendicular to the directions ξ and $-\xi$, Figure 3. In further considerations, a single set of the bands with the orientation ξ is considered.[3] In each band the increments $\hat\gamma^{(1)}$, $\hat\gamma^{(2)}$ and $\hat\omega^*$ are supposed to be uniform. Slip is adjusted such that in the direction perpendicular to the bands the incremental slips alternate and is averaged to zero, i.e. $\Delta\hat\gamma^{(i)} = 2\hat\gamma^{(i)}$. The width $L > 0$ of the bands is taken to be the same for all the bands.

Upon introducing the stream function using relations (8) evaluated for the considered microstructure ξ of Figure 3 with $\Delta\hat\gamma^{(i)} = 2\hat\gamma^{(i)}$, the functional (25) becomes

$$J_c = \frac{1}{2}\left(4\left[H_{xx} + B_{xx}\right]\xi^2 + \left[H_{xy} + B_{xy}\right]\left(\xi^2 - 1\right)^2 - \frac{\bar\sigma}{2}\left(1 - \xi^4\right)\right)\int_\Omega \left(F''\right)^2 {\rm d}V + \left(4\tilde H_{xx}\xi^2 + \tilde H_{xy}\left(1 - \xi^2\right)^2\right)\int_A \left(F''\right)^2 {\rm d}A\,, \tag{26}$$

where H_{xx} and H_{xy} are given by (15), and

$$\tilde H_{xx} = \frac{\tilde h(1+\tilde q)}{2\sin^2 2\phi}\,, \quad \tilde H_{xy} = \frac{\tilde h(1-\tilde q)}{2\cos^2 2\phi}\,, \quad B_{xx} = \frac{h_{\rm bow}}{2\sin^2 2\phi}\,, \quad B_{xy} = \frac{h_{\rm bow}}{2\cos^2 2\phi}\,. \tag{27}$$

The functional (26) for the neglected length-scale effects, $h_{\rm bow} = 0$ and $\hat h = 0$ is reduced to the functional (19) of the simple model.

In view of that the area A of all GNBs in the volume V of Ω is V/L, the shear strain in the bands $F'' = \pm(a/L)$, where a is an amplitude of the incremental displacement and that we assume $h_{\rm bow} = Gb/L$ the functional J_c becomes the energetic function

$$J_c(\xi, L) = \frac{1}{2}\left(4H_{xx}\xi^2 + H_{xy}\left(\xi^2 - 1\right)^2 - \frac{\bar\sigma}{2}\left(1 - \xi^4\right)\right)\frac{a^2}{L^2}V + \left(4\left[\tilde H_{xx} + B_{xx}\right]\xi^2 + \left[\tilde H_{xy} + B_{xy}\right]\left(1 - \xi^2\right)^2\right)\frac{a^2}{L^3}V\,. \tag{28}$$

Note that the function (28) for $h_{\rm bow} = 0$ and $\hat h = 0$ is identical to $J(L, \xi)$ of the length-scale estimate (22) of the simple model.

The reduced energetic function $\bar J_c(L, \xi) = J_c/H_{xx}Va^2$ can be expressed as

$$\bar J_c\,(\xi, L) = \frac{1}{L^2}\left[2\xi^2 + K\left(1 - \xi^2\right)^2 + S\left(1 - \xi^4\right)\right] + \frac{2}{L^3}\left[M\xi^2 + N\left(1 - \xi^2\right)^2\right], \tag{29}$$

where K and S are given by (21) and

$$M = 2\frac{\tilde{H}_{xx} + B_{xx}L/2}{H_{xx}} = \frac{2\tilde{h}(1+\tilde{q}) + Gb}{h(1+q)}\,, \tag{30a}$$

$$N = \frac{\tilde{H}_{xy} + B_{xy}L/2}{2H_{xx}} = \frac{2\tilde{h}(1-\tilde{q}) + Gb}{4h(1+q)}\tan^2 2\phi\,. \tag{30b}$$

The minimum of the reduced energetic function $\bar{J}_c(L,\xi)$ with respect to the width L and the orientation ξ indicates the most favourable structure formed. The conditions of the minimum are: $\partial\bar{J}_c/\partial L = 0$ and $\partial\bar{J}_c/\partial\left(\xi^2\right) = 0$.

For the band orientation ξ evaluated by the minimisation of $\bar{J}_c$ the dislocation composition of GNBs is given by (9) where F''' is of the form of δ-function. If the orientation of the boundaries would coincide with the one of the slip planes, e.g. $\xi > 0$ requiring $\xi = -\tan\phi$, both $\hat{\alpha}^{(i)}$ are zero. This is understandable as the shear deformation is carried fully by compatible slip $\hat{\gamma}^{(2)}$. The misorientation across GNBs can be evaluated from (10) with $F'' = \pm a/L$; the amplitude a is not specified by the present rate independent version of the model, a rate dependent version would indicate a growth of a.

3. Results and discussion

The minimisation of the reduced energetic function $\bar{J}_c(L,\xi)$ expressed by (29) is an easy task.[4] To estimate values of the parameters K, S, M and N for a material in a given strain stage is more difficult. As seen from (21) and (30) these parameter are controlled by: the self-hardening h, the latent-to-self hardening ratio q (the anisotropy factor), the flow stress $\bar{\sigma}$, the shear modulus G, the magnitude of the Burgers vector b, the boundary slip resistance $\tilde{h}$ and the slip resistance anisotropy $\tilde{q}$. For a given material at a given strain, h and $\bar{\sigma}$ can be estimated from the stress–strain diagram. At small strains, the value of the ratio q is usually taken $q \sim 1.4$; to our knowledge, for medium and large strains q is not known. One can only safely assume that $q > 1$, as for all strains a local decrease in the number of the active slip systems controlled by q is energetically favourable. G and b are known constants, however, the assumption that the line tension strengthening $h_{\mathrm{bow}} = Gb/L$ which modifies h is a result of an intuition rather than a rationally deduced consequence of the bowing mechanism. We have not found any guideline for an estimate of the slip resistance coefficients $\tilde{h}$ and $\tilde{q}$, therefore, they enter the model as fitting parameters. Attempts to quantify the grain boundary interface mechanisms faced analogical problems [41]).

To demonstrate the predictive ability of the model two examples are presented: the deformation bands formed in Ni at the moderate strain $\varepsilon = 0.5$ and at the large strain $\varepsilon = 2.5$. Due to several simplifying assumptions numerical data predicted by the model are just indicative.

At the moderate strain $\varepsilon = 0.5$ the self-hardening $h = 400\,\mathrm{MPa}$ and the compressive flow stress $\bar{\sigma} = -500\,\mathrm{MPa}$ were deduced for Ni from the stress–strain diagram in [4] (Fig. 14); for nickel $G \sim 70$ GPa and $b = 0.25$ nm, i.e. $Gb = 17\,\mathrm{MPa\,\mu m}$; we use the hardening anisotropy ratio $q = 1.5$. A few illustrative values of the boundary resistance $\tilde{h}$ and the resistance anisotropy $\tilde{q}$ employed as the fitting parameters are listed in Table 1 together with the values of the angle θ_{roll} and the band width L which correspond for these values to the minimum of the reduced energetic function $\bar{J}_c$. The graph of $\bar{J}_c(\xi)$ for L=1 μm , $\tilde{h}$=145 MPa μm and $\tilde{q} = 2.5$ is plotted as an example in Figure 5 for the

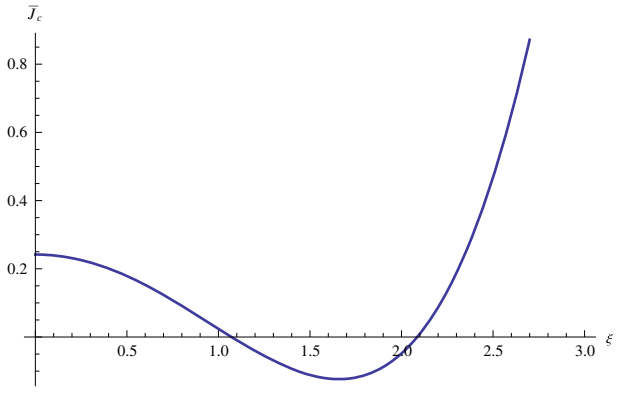

Figure 5. (colour online) Graph of the reduced energetic function $\bar{J}_c(L, \xi)$ evaluated for $L = L_{\min}$.

Table 1. Model parameters of the deformation band structure at moderate strains $\varepsilon = 0.5$.

θ_{roll}	L [μm]	$\tilde{h}$ [MPa μm]	$\tilde{q}$
30°	1.2	−172	2.57
30°	1	−145	2.53
30°	0.8	−117	2.50
25°	1.2	−357	1.80
25°	1	−249	1.79
25°	0.8	−241	1.79

Table 2. Model parameters of the deformation band structure at large strains $\varepsilon = 2.5$.

θ_{roll}	L [μm]	$\tilde{h}$ [MPaμm]	$\tilde{q}$
10°	0.3	−963	1.065
10°	0.2	−627	1.059
10°	0.1	−318	1.045
5°	0.3	−4214	1.014
5°	0.2	−2812	1.013
5°	0.1	−1410	1.011

comparison to the graph of the simple model in Figure 4. The values of the band width L and the inclination angle θ_{roll} correspond roughly to the measured values presented in [42] $L \sim 1.5\,\mu\text{m}$ (deduced from the graph Figure 3 in [42]) and the observed $\theta_{\text{roll}} \sim 30°$ [10]. In the example of the moderate strain, $\tilde{h}$ and $\tilde{q}$ are the factors controlling the orientation and the width of the bands. As can be deduced from Table 1 the boundary resistance $\tilde{h}$ influences mainly the width L and the resistance anisotropy $\tilde{q}$ controls the inclination angle θ_{roll}.

The negative sign of $\hat{h}$ seen in Tables 1 and 2 indicates that the boundary part of the hardening rule (24) represents a back stress. This is understandable as the excess dislocations in the GNBs produce long-range stresses. An analogical situation arose in the attempt [43] to explain the high anisotropy and the stress–strain behaviour observed in metallic films having strongly non-equiaxed grains (an analogy of the quasi-parallel deformation bands with extended planar GNBs). To explain these observations, the authors of [43] had to introduced in the flow rule a back stress (an analogy of $\hat{h}$) and a strong anisotropy factor (an analogy of $\hat{q}$).

The dislocation composition of the GNBs is represented by $\hat{\alpha}^{(i)}$ given by (9). In the example $\varepsilon = 0.5$ the orientation of the GNBs deviates from the orientation of the nearest slip system (characterised by $-\phi = -35^\circ$ and $\hat{\alpha}^{(2)}$) by 25°. The evaluated composition ratio $\left|\hat{\alpha}^{(1)}\right| / \left|\hat{\alpha}^{(2)}\right| = 11.5$ indicates that the composition is dominated by the dislocations from the other slip system ($\phi = 35^\circ$ and $\hat{\alpha}^{(1)}$). For comparison the ratio $|\hat{\alpha}^{(1)}|/|\hat{\alpha}^{(2)}|$ of the coplanar densities can be deduced from unique experimental data presented in [13] (Table 2 and Figure 11) for Al reduced by rolling 10% ($\varepsilon \sim 0.1$). The experimentally determined averaged composition ratio is ∼10 for the deviations ∼5°, it decreases to ∼1 at the deviations ∼15°, and then it becomes less than 1.

At the large strain $\varepsilon = 2.5$ we use the self-hardening $h = 60$ MPa and the compressive flow stress $\bar{\sigma} = -700$ MPa deduced for Ni from [4] (Fig. 14) and the hardening anisotropy ratio $q = 1.5$. A few illustrative values of the fitting parameters $\tilde{h}$ and $\tilde{q}$ are listed in Table 2 together with the values of the angle θ_{roll} and the band width L for the minimum of the reduced energetic function $\bar{J}_c$. The shape of the graph of $\bar{J}_c(L, \xi)$ for $L = L_{\min}$, not presented here, is similar to the graph in Figure 5 only the minimum value is shifted to higher value of ξ. The predicted values of the band width L and the inclination angle θ_{roll} correspond roughly to the observed trend of a decreasing band width and the reorientation of the bands toward the RD. The higher values of $\tilde{h}$ and $\tilde{q}$ approaching 1 indicate an increasing resistance of the boundaries and its isotropy contributing to the tendency to orient the bands parallel to the RD $\xi \to \infty$ and to reach a zero width. As a consequence, the controlling factor at the large strain becomes the bowing stress represented by h_{bow} which prevents these extremes. The dislocation composition of the GNBs at $\theta_{\text{roll}} = 10^\circ$ represented by the ratio $\left|\hat{\alpha}^{(1)}\right| / \left|\hat{\alpha}^{(2)}\right| \sim 2$.

A comparison of Tables 1 and 2 reveals a significant change of $\hat{h}$ and $\hat{q}$ with increasing strain. The change is probably caused by the observed formation of the MBs at the boundaries which replace the original DDWs. This transformation could cause radical changes in mechanical properties of the modified GDBs indicated by the change in $\hat{h}$ and $\hat{q}$. As a consequence, the CBs are transformed into the energetically more favourable lamellar structure. Moreover, according to the observations [10], the S-bands play in a mechanism of the CBs-lamellae transformation a key role. The symmetry of the MBs and the S-bands with respect to the compression axis indicated in the sketch in Fig. 14 in [10] suggests that the MBs and S-bands are a pair of the equally energetically favourable deformation bands of the orientations $\pm\xi$, Figure 3, as predicted by the presented model.

It is interesting to note that the shape of the reduced energetic function at the minimum is rather flat, as seen in Figure 5. This indicates that the deformation bands of the width L and the orientation ξ close to the values at the minimum may appear. This corresponds to the observed scatter in these parameters.

4. Summary

Positive aspects:

- The model represents a unified approach which provides an explanation of the process of the fragmentation in the form of the deformation bands. The model points to the main ingredients which control the fragmentation mechanism: the anisotropy of the hardening matrix, the anisotropic resistance of the boundaries to slip and the bowing stress.
- The deformation bands (internal buckling) are spontaneously formed due to strong anisotropy caused by the slip nature of plastic deformation.
- The proposed model predicts in the plain-strain approximation the band orientation, their width and the dislocation composition of the band boundaries.
- The significant change in the structural morphology with increasing strain, i.e. the reorientation of the bands from $\sim 30^\circ$ to nearly 0° with respect to the RD, is interpreted as the transition from the boundary control bands formation to the bowing stress control.
- Due to the line character of glide dislocations accompanied by the line tension, the bands cannot be exactly parallel to the RD and their width cannot reach zero.

Drawbacks and open questions:

- The coefficients $\tilde{h}$ and $\tilde{q}$ representing the energy contribution of the boundaries serve as the fitting parameters. The assumption that the line tension strengthening $h_{\mathrm{bow}} = Gb/L$ modifies the self-hardening h is rather intuitive.
- The model does not explain the observed transformation of the DDWs to the MBs.
- The role of the inner structure of the bands (cells, Taylor lattice) and the sharp or diffuse shapes of the boundaries remains an open problem.

Disclosure statement

No potential conflict of interest was reported by the authors.

Funding

This work was supported by GAČR through project P107/12/0121.

Notes

1. The parameter ξ could be equally well placed by its inverse at x resulting in an equivalent formulation. The chosen form of the stream function (6) leads to a direct connection of ξ to the orientation of the deformation bands θ_{roll} with respect to the RD, $\theta_{\mathrm{roll}} = \pi/2 - \arctan \xi$.
2. Expressing formally the boundary part in terms of δ-function at the positions of the GNBs the functional J_c can be formulated as a single volume integral over Ω.
3. A generalization to two sets is straightforward; a probable reason that two criss-crossing sets are less frequently observed is an interaction between sets not covered by the present linearised model.
4. By MATHEMATICA (http//www.wolfram.com) the values of L_{min} and ξ_{min} at the minimum can be reach even in an analytical but rather complicated form.

References

[1] B. Bay, N. Hansen, D.A. Hughes and D. Kuhlmann-Wilsdorf, Acta Metall. Mater. 40 (1992) p.205.
[2] D. Kuhlmann-Wilsdorf, Acta Mater. 47 (1999) p.1697.
[3] D.A. Hughes, Mater. Sci. Eng. A319–321 (2001) p.46.
[4] N. Hansen and D. Juul Jensen, Mater. Sci. Technol. 27 (2011) p.1229.
[5] M.A.Biot, *Mechanics of Incremental Deformations*, Willey, New York, 1965,
[6] R. Hill and J.W. Hutchinson, J. Mech. Phys. Solids 23 (1975) p.2396.
[7] R.J. Asaro, Adv. Appl. Mech. 23 (1983) p.1.
[8] C.S. Hong, X. Huang and G. Winther, *Experimental characterization of dislocations in deformation induced planar boundaries of rolled aluminium*, in *Proceedings of the 33rd Risoe International Symposium on Material Science: Nanometals – Status and Perspective*, S. Fæster, N. Hansen, X. Huang, D. Juul Jensen and B. Ralph, eds., Risoe National Laboratory, Roskilde, 2012, pp.239–248.
[9] D.A. Hughes, Acta Metall. Mater. 41 (1993) p.1421.
[10] D.A. Hughes and N. Hansen, Metall. Trans. A 24 (1993) p.2021.
[11] D.A. Hughes and N. Hansen, Acta Mater. 48 (2000) p.2985.
[12] D.A. Hughes, Q. Liu, D.C. Chrzan and N. Hansen, Acta Mater. 45 (1997) p.105.
[13] C. Hong, X. Huang and G. Winther, Philos. Mag. 93 (2013) p.3118.
[14] S.V. Harren, H.E. Dève and R.J. Asaro, Acta Metall. 36 (1988) p.2435.
[15] J. Kratochvíl and A. Orlová, Philos. Mag. A 61 (1990) p.281.
[16] J. Kratochvíl, Scr. Metall. Mater. 24 (1990) p.1225.
[17] J. Kratochvíl, M. Kružík and R. Sedláček, Acta Mater. 57 (2009) p.739.
[18] R. Sedláček and J. Kratochvíl, Z. Metallkd. 96 (2005) p.602.
[19] J. Kratochvíl and R. Sedláček, Mater. Sci. Eng. A387–389 (2004) p.67.
[20] J. Kratochvíl, M. Kružík and R. Sedláček, Phys. Rev. B 75 (2007) p.064104.
[21] H. Petryk and M. Kursa, J. Mech. Phys. Solids 61 (2013) p.1854.
[22] R. Hill, J. Mech. Phys. Solids 14 (1966) p.95.
[23] R. Hill and J.R. Rice, J. Mech. Phys. Solids 20 (1972) p.401.
[24] D. Peirce, R.J. Asaro and A. Needleman, Acta Metall. 31 (1983) p.1951.
[25] J.L. Bassani, Adv. Appl. Mech. 30 (1994) p.191.
[26] M. Ortiz and E.A. Repetto, J. Mech. Phys. Solids 47 (1999) p.397.
[27] M. Ortiz, E.A. Repetto and L. Stainer, J. Mech. Phys. Solids 48 (2000) p.2077.
[28] S. Aubry and M. Ortiz, Proc. R. Soc. London A 459 (2003) p.3131.
[29] H. Petryk, J. Mech. Phys. Solids 40 (1992) p.1227.
[30] H. Petryk, J. Mech. Phys. Solids 48 (2000) p.367.
[31] H. Petryk and K. Thermann, J. Mech. Phys. Solids 50 (2002) p.925.
[32] H. Petryk and M. Kursa, Arch. Mech. 63 (2011) p.287.
[33] X. Huang and G. Winther, Philos. Mag. 87 (2007) p.5189.
[34] G. Winther and X. Huang, Philos. Mag. 87 (2007) p.5215.
[35] S. Mahesh, Philos. Mag. 92 (2012) p.2286.
[36] G. Winther, *Theoretical analysis of slip-plane-aligned geometrically necessary dislocation boundaries originating from two sets of coplanar slip systems*, in *Proceedings of the 33rd Risoe International Symposium on Material Science: Nanometals – Status and Perspective*, S. Fæster, N. Hansen, X. Huang, D. Juul Jensen and B. Ralph, eds., Risoe National Laboratory, Roskilde, 2012, pp.115–128.
[37] G. Winther, C.S. Hong and X. Huang, *Comparison of experimental and predicted dislocation network in deformation-induced dislocation boundaries aligned with slip planes in aluminium*, in *Proceedings of the 35th Risoe International Symposium on Material Science: New Frontiers*

of Nanometals, S. Fæster, N. Hansen, D. Juul Jensen, B. Ralph and J. Sun, eds., Technical University of Denmark, Roskilde, 2014, pp.479–484.
[38] T. Leffers, Int. J. Plast. 17 (2001) p.469.
[39] T. Leffers, Int. J. Plast. 17 (2001) p.491.
[40] J. Kratochvíl and M. Kružík, *A model of deformation bands formation*, in *Proceedings of the 35th Risoe International Symposium on Material Science: New Frontiers of Nanometals*, S. Fæster, N. Hansen, D. Juul Jensen, B. Ralph and J. Sun, eds., Technical University of Denmark, Roskilde, 2014, pp.357–364.
[41] P.R.M. van Beers, G.J. McShane, V.G. Kouznetsova and M.G.D. Geers, J. Mech. Phys. Solids 61 (2013) p.2659.
[42] D.A. Hughes, *Distribution of low and high angle boundaries in deformed metal*, in *Proceedings of the Fourth Conference on Recrystalization and Related Phenomena*, T. Sakai and H.G. Suzuki, eds., The Japan Institute of Metals, Sendai, 1999, pp.111–118.
[43] L. Delannay and M.R. Barnett, Int. J. Plast. 32–33 (2012) p.70.